Cascade Viscous Flow Analysis Using the Navier-Stokes Equations

Roger L. Davis,* Ron-Ho Ni,† and James E. Carter‡
United Technologies Corporation, East Hartford, Connecticut

A previously developed explicit, multiple-grid, time-marching Navier-Stokes solution procedure has been modified and extended for the calculation of steady-state high Reynolds number turbulent flows in cascades. Particular attention has been given to the solution accuracy of this procedure as compared with boundary-layer theory and experimental data. A new compact discretization scheme has been implemented for the viscous terms which has the same finite-difference molecule as the inviscid terms of the Navier-Stokes equations. This compact operator has been found to yield accurate and stable solutions in regions of the flow where the gradients are large and the computational mesh is relatively sparse. A modified C grid generation procedure has been developed for cascades that greatly reduces grid skewing in the midgap region. As a result, numerical errors associated with the use of numerical smoothing on skewed grids are reduced considerably. In addition, a body normal grid system has also been generated for accurately determining the eddy viscosity distribution based on an algebraic turbulence model and for comparing the results directly with boundary-layer theory. A combined second and fourth difference numerical smoothing operation has been carefully constructed to prevent oscillations in the solution for the flow over complicated geometries without contaminating the velocity profiles near the wall. Results from turbine and compressor applications are presented to demonstrate the accuracy of the present scheme through comparisons with experimental data and attached boundary-layer theory.

Nomenclature

c = speed of sound
C_p = specific heat at constant pressure
C_v = specific heat at constant volume
e = specific internal energy
E = total energy
h = static enthalpy
H = stagnation enthalpy or streamtube height
M = Mach number
N = normal distance from airfoil surface
P = static pressure
Pr = Prandtl number
Pr_T = turbulent Prandtl number
P_T = stagnation pressure
R = gas constant
Re = Reynolds number based upon unit length
S_t = Stanton number
T = static temperature
T_T = stagnation temperature
t = time
u = axial (x) component of velocity
v = tangential (y) component of velocity
V = velocity
$\mathcal{V}$ = volume of computational cell
x = axial component of Cartesian coordinate system
y = tangential component of Cartesian coordinate system
β = air angle relative to tangential
ϵ = turbulent eddy viscosity coefficient
γ = ratio of specific heats, C_P/C_v
μ = kinematic viscosity coefficient
ρ = density
ψ = smoothing coefficient

Subscripts

1 = inlet
2 = exit
INV = inviscid
VIS = viscous

Introduction

THE drive toward higher jet engine efficiency has resulted in increased aerodynamic and heat-transfer demands on the compressor and turbine sections of gas turbine engines. As loading requirements in the blade rows and turbine inlet stagnation temperatures increase beyond the range of previous applications, the designer's job becomes increasingly difficult without the use of sophisticated three-dimensional flow analyses. Separated flow regions and hot spots in turbomachinery blade passages occur more frequently as the operation envelope is pushed to the limit. In order to determine the existence and effects of these phenomena, an accurate and reliable three-dimensional viscous flow procedure becomes necessary.

The analysis and prediction of three-dimensional viscous flows in blade rows have only recently been treated in the literature.[1-3] Severe demands are placed on computer storage and computational time in order to resolve accurately the wall layers adjacent to the airfoil surface and endwalls. A logical starting point for the eventual development of a three-dimensional viscous analysis for turbomachinery is the development of a two-dimensional solution technique for the Navier-Stokes equations in which the wall layers are resolved with fine grid distributions. Recent advances in multiple-grid and implicit procedures have led to the development of several two-dimensional cascade Navier-Stokes techniques.[4-7] The overall objective of the present investigation is the development of a cascade Navier-Stokes solution procedure based on the Ni[8] Euler technique which gives good agreement with experimental data and finite-difference, boundary-layer calculations for attached flows.

Presented as Paper 86-0033 at the AIAA 24th Aerospace Sciences Meeting, Reno, NV, Jan. 6-9, 1986; received Feb. 19, 1986; revision received Dec. 2, 1986. Copyright © American Institute of Aeronautics and Astronautics, Inc., 1987. All rights reserved.

*Research Engineer, United Technologies Research Center. Member AIAA.

†Senior Research Engineer, Pratt & Whitney Aircraft. Member AIAA.

‡Manager, Computational Fluid Dynamics, United Technologies Research Center. Member AIAA.

The present solution technique for the two-dimensional Navier-Stokes equations is a modification and extension of the one-step control volume algorithm presented by Davis et al.[9] This algorithm uses an explicit, control volume approach combined with an efficient multiple-grid scheme[8,9] to update the flow variables in time until a steady-state solution is obtained. The solution procedure is formally second-order accurate in space for all terms in the Navier-Stokes equations. The present time-marching scheme is second-order accurate in time for inviscid flow and first-order accurate in time for viscous flow which is similar to previous efforts.[10-12] Several modifications and improvements in this Navier-Stokes solution technique have been made in the present investigation to allow for the calculation of turbulent, high Reynolds number flow in cascades. A new compact operator for the calculation of the viscous terms in the Navier-Stokes equations has been developed which improves the accuracy and stability of the numerical approach. A modified C grid generation procedure, developed in collaboration with Dannenhoffer[13] and based upon the "GRAPE" Poisson solver of Sorenson[14] and Steger and Sorenson,[15] has been found to greatly reduce the computational grid skewing in the midpassage region compared to standard cascade C grid applications, thereby reducing numerical losses introduced by smoothing operators applied on skewed grids. The Baldwin-Lomax[16] two-layer algebraic turbulence model has been implemented using a body normal grid that alleviates any *a priori* approximations as to the thickness of the boundary-layer region adjacent to the solid surface. A combination of second and fourth difference numerical smoothing is used in the present numerical procedure to dampen oscillations brought about by truncation errors on relatively coarse grids. Both second and fourth difference smoothing operators for the flow variables ρu and ρv are reduced to zero as the solid boundary is approached in order to accurately resolve the viscous layer region.

Analysis

Navier-Stokes Solution Procedure

The technique described in this paper is an explicit, time-marching, control volume scheme. The time-dependent, Reynolds-averaged Navier-Stokes equations are integrated around small discrete quasi-three-dimensional control volumes defined by the computational mesh and streamtube height distribution to give the time rate change of the flow variables. The time rate change of the flow variables is multiplied by the appropriate local time step and the flow variables are then updated in time. A multiple-grid algorithm is used to accelerate convergence to a steady-state solution.

Governing Equations

The two-dimensional Navier-Stokes equations are solved in conservative form in a Cartesian coordinate system for cases without blade rotation or radius change effects. In cases which include blade rotation or radius change effects, the Navier-Stokes equations are solved in conservative form in the cylindrical coordinate system along a cone with a linearly varying radius between the leading and trailing edge of the cascade. The quasi-three-dimensional effects due to varying streamtube height are included in either coordinate system. For the sake of simplicity, only the Navier-Stokes equations in Cartesian form will be presented here. The Navier-Stokes equations as solved in the present procedure are given as

$$\frac{\partial U}{\partial t}+\frac{\partial (F_1+F_2)}{\partial x}+\frac{\partial (G_1+G_2)}{\partial y}=0 \tag{1}$$

where

$$U=\begin{bmatrix}\rho\\ \rho u\\ \rho v\\ E\end{bmatrix} \quad F_1=\begin{bmatrix}\rho u\\ \rho u^2+P\\ \rho uv\\ \rho uH\end{bmatrix} \quad F_2=-\begin{bmatrix}0\\ \tau_{xx}\\ \tau_{xy}\\ \tau_{hx}\end{bmatrix}$$

$$G_1=\begin{bmatrix}\rho v\\ \rho uv\\ \rho v^2+P\\ \rho vH\end{bmatrix} \quad G_2=-\begin{bmatrix}0\\ \tau_{xy}\\ \tau_{yy}\\ \tau_{hy}\end{bmatrix}$$

and

$$\tau_{xx}=\mu\left(1+\frac{\epsilon}{\mu}\right)\left(\frac{4}{3}\frac{\partial u}{\partial x}-\frac{2}{3}\frac{\partial v}{\partial y}\right)$$

$$\tau_{yy}=\mu\left(1+\frac{\epsilon}{\mu}\right)\left(\frac{4}{3}\frac{\partial v}{\partial y}-\frac{2}{3}\frac{\partial u}{\partial x}\right)$$

$$\tau_{xy}=\mu\left(1+\frac{\epsilon}{\mu}\right)\left(\frac{\partial u}{\partial y}+\frac{\partial v}{\partial x}\right)$$

$$\tau_{hx}=\frac{\mu}{Pr}\left(1+\frac{\epsilon}{\mu}\frac{Pr}{Pr_T}\right)\frac{\partial H}{\partial x}+\mu\left\{u\left[\left(\frac{4}{3}-\frac{1}{Pr}\right)\frac{\partial u}{\partial x}-\frac{2}{3}\frac{\partial v}{\partial y}\right]+v\left[\frac{\partial u}{\partial y}+\left(1-\frac{1}{Pr}\right)\frac{\partial v}{\partial x}\right]\right\}$$

$$\tau_{hy}=\frac{\mu}{Pr}\left(1+\frac{\epsilon}{\mu}\frac{Pr}{Pr_T}\right)\frac{\partial H}{\partial y}+\mu\left\{v\left[\left(\frac{4}{3}-\frac{1}{Pr}\right)\frac{\partial v}{\partial y}-\frac{2}{3}\frac{\partial u}{\partial x}\right]+u\left[\left(1-\frac{1}{Pr}\right)\frac{\partial u}{\partial y}+\frac{\partial v}{\partial x}\right]\right\}$$

In addition,

$$E=\rho[e+\tfrac{1}{2}(u^2+v^2)] \qquad H=h+\tfrac{1}{2}(u^2+v^2)$$
$$P=\rho RT \qquad H=(E+P)/\rho \tag{2}$$

For adiabatic flows, the energy equation is replaced by

$$H=\text{const} \tag{3}$$

For a perfect gas

$$h=C_pT \qquad e=C_vT$$
$$C_p=\gamma R/(\gamma-1) \qquad C_v=R/(\gamma-1) \tag{4}$$

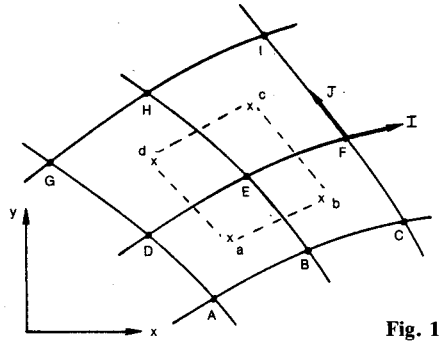

Fig. 1 Computational cell.

Sutherland's law is used to relate the coefficient of viscosity to the static temperature for air. The turbulent eddy viscosity is obtained from the Baldwin-Lomax[16] two-layer, algebraic turbulence model as will be discussed later.

The local time step used in this procedure is determined from the CFL and diffusion limitations described by Richtmyer and Morton[17] as follows:

$$\Delta t = \min\left(\frac{\Delta L}{|V\cdot 1| + c + (\alpha\tilde{\mu}/\Delta L)}\right) \tag{5}$$

where L is the streamwise or tangential direction across the control volume, 1 the unit vector along L, $\tilde{\mu}$ the total viscosity coefficient given by

$$\tilde{\mu} = \mu + \epsilon + \hat{\mu} \tag{6}$$

and $\hat{\mu}$ an estimate of the artificial viscosity coefficient due to the second and fourth difference numerical smoothing performed, which will be described later. The coefficient α is the inverse of the diffusion number and has been set equal to 8.0 based upon numerical results.

Boundary Conditions

The total pressure and total temperature are either held constant or at a prescribed distribution at the upstream boundary of the cascade, which is usually located 75% of the axial chord upstream of the leading edge. The average air angle is also held fixed at the upstream boundary by redefining the local time rate changes in the velocity components to be proportional to the difference between the average inlet air angle at the new time level and the inlet air angle which is to be held. The local time rate changes in the density and energy are then redefined using Eq. (2) in order to hold the inlet total pressure and total temperature. At the downstream boundary, which is usually located 75% of the axial chord downstream of the trailing edge, the average static pressure is held when the flow is subsonic. This is performed by redefining the local time rate changes in the density and energy using Eq. (2) to be proportional to the difference between the average exit static pressure at the new time level and the exit static pressure that is to be held. The advantage of holding the average static pressure at the downstream boundary as opposed to a constant static pressure condition is that local variations in the static pressure may occur without incurring a change in the mass flow rate. This relieves feedback of pressure waves into the computational domain, especially as the "start-up" vortex passes through the downstream boundary. When the exit flow is supersonic, a radiation condition[9] is used at the downstream boundary. A no-slip boundary condition is used at the solid boundaries and, for nonadiabatic flows, a wall stagnation temperature distribution is prescribed. In addition, a transpiration boundary condition is allowed at the wall to model film cooling effects or boundary-layer suction. A periodicity condition is used along the wake centerline and at the outer boundary of the computational C grid in the midgap region of the cascade passage.

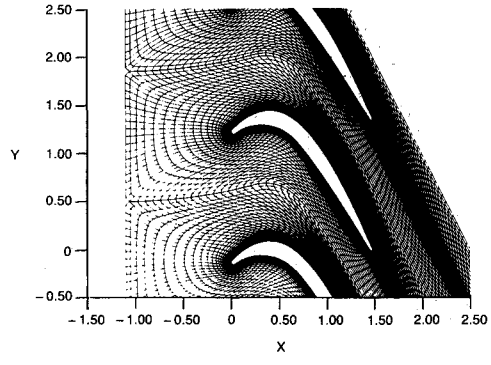

Fig. 2a Standard C grid.

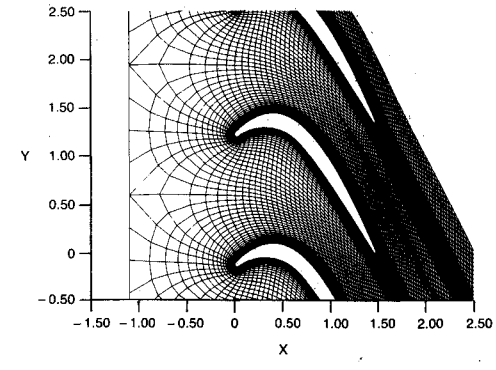

Fig. 2b Modified C grid.

Numerical Scheme

The numerical technique used to obtain a steady-state solution of the Navier-Stokes equations consists of an extension of the explicit Ni[8] multiple-grid scheme originally used for the solution of the Euler equations. In a previous effort,[9,10] the algorithm developed by Ni was extended to the solution of the Navier-Stokes equations for laminar flows. In this technique, the procedure of updating the flow variables of U in time was performed according to a second-order accurate Taylor series expansion given by

$$U^{t+\Delta t} = U^t + \frac{\partial U}{\partial t}\Delta t + \frac{\partial^2 U}{\partial t^2}\frac{\Delta t^2}{2} \tag{7}$$

The viscous stress and conduction terms of the Navier-Stokes equations were calculated using central difference formulas and stored at the computational nodes (i.e., at A through I in Fig. 1) and, as such, were included in the integration step which determined the first-order time rate change of the flow variables at the primary control volume centers (i.e., at a through d in Fig. 1). For instance, at cell center c in Fig. 1,

$$\left.\frac{\partial U}{\partial t}\right|_c = \frac{1}{\mathcal{V}}\int_{\text{EFIH}}\left[\frac{\partial(F_1+F_2)}{\partial x} + \frac{\partial(G_1+G_2)}{\partial y}\right]d\mathcal{V} \tag{8}$$

Subsequently, these time rate changes are computed and distributed to the computational nodes using the Ni distribution formula[8] which consists of two basic operations. The first operation determines the first-order time rate change at the computational nodes by averaging the surrounding primary control volume center values (i.e., at a through d) as given, for example at E, by

$$\left.\frac{\partial U}{\partial t}\right|_E = \frac{1}{4}\sum_{k=\text{abcd}}\frac{\partial U}{\partial t}k \tag{9}$$

The second operation determines the second-order time rate change at the computational nodes through a piecewise integration of the time derivative of the Navier-Stokes equations around a secondary control volume that has its corners at the surrounding primary control volume centers. This operation is written as follows for node E:

$$\left.\frac{\partial^2 U}{\partial t^2}\right|_E = \frac{1}{\mathcal{V}}\int_{\text{abcd}}\frac{\partial}{\partial t}\left[\frac{\partial(F_1+F_2)}{\partial x} + \frac{\partial(G_1+G_2)}{\partial y}\right]d\mathcal{V} \tag{10}$$

This approach is similar to Ni's solution procedure except that the Navier-Stokes equations are substituted for the Euler equations. Thus, the viscous shear stress and conduction terms affect both the first- and second-order time rate changes at the

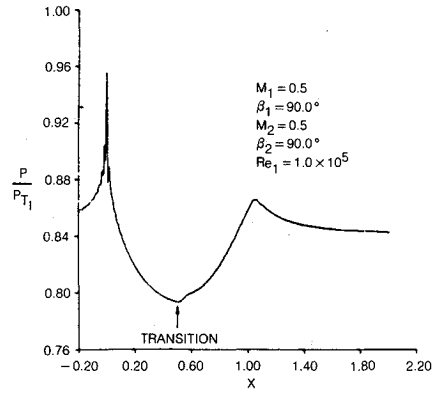

Fig. 3a Predicted pressure distribution for 10% circular arc cascade.

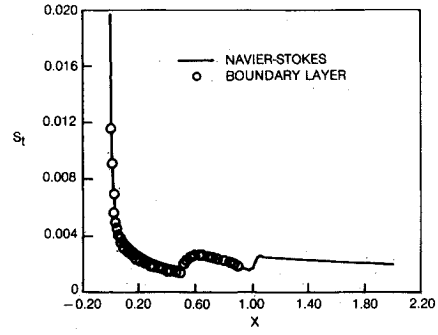

Fig. 3b Predicted Stanton number distribution for 10% circular arc cascade.

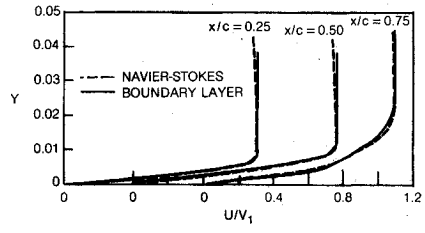

Fig. 3c Predicted velocity profiles for 10% circular arc cascade.

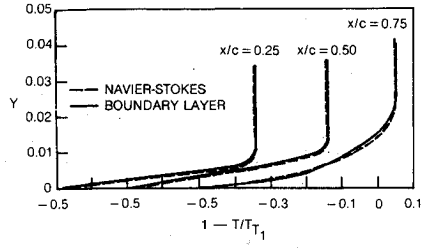

Fig. 3d Predicted temperature profiles for 10% circular arc cascade.

computational nodes with this scheme. The domain of influence of the viscous terms on a given computational node in this approach includes information from its surrounding 25 nodes or 2 computational cells in each direction. Even though second-order temporal and spatial accuracy is maintained with this approach, solutions for cascade geometries have been found to exhibit oscillations in high gradient regions near the leading and trailing edges. These oscillations are thought to be due in part to the truncation error introduced by the large domain of influence on each node. In order to alleviate these oscillations, a new compact discretization technique for the viscous terms in the Navier-Stokes equations was developed that reduces the domain of influence on a computational node to include information from only its 9 surrounding nodes.

In the new approach, the viscous shear stress and conduction terms in the Navier-Stokes equations have been uncoupled from the "distribution formula" of the original scheme[9] used to distribute biased time rate changes of the flow variables from the control volume centers to the computational nodes. In this new procedure, the method of updating the flow variables of U in time is performed according to the formula

$$U^{t+\Delta t} = U^t + \left(\left.\frac{\partial U}{\partial t}\right|_{\text{INV}} + \left.\frac{\partial U}{\partial t}\right|_{\text{VIS}}\right)\Delta t + \left.\frac{\partial^2 U}{\partial t^2}\right|_{\text{INV}} \frac{\Delta t^2}{2} \tag{11}$$

The Euler equations are integrated around the primary control volumes such as EFIH in Fig. 1, defined by the computational grid, to give the inviscid first-order changes in time of the flow variables at the control volume centers (i.e., at c in Fig. 1).

$$\left.\frac{\partial U}{\partial t}\right|_{\substack{\text{INV}\\ \text{c}}} = \frac{1}{\mathcal{V}} \int_{\text{EFIH}} \left(\frac{\partial F_1}{\partial x} + \frac{\partial G_1}{\partial y}\right) d\mathcal{V} \tag{12}$$

The inviscid flow variable first-order changes in time at the computational nodes (i.e., at E), are calculated from an averaging of the surrounding control volume center inviscid first-order time rate changes (i.e., at a,b,c, and d) as part of the distribution formula.[8]

$$\left.\frac{\partial U}{\partial t}\right|_{\substack{\text{INV}\\ \text{E}}} = \frac{1}{4} \sum_{k=\text{abcd}} \left.\frac{\partial U}{\partial t} k\right|_{\text{INV}} \tag{13}$$

The contribution of the inviscid terms to the second-order changes in time of the flow variables are included in the distribution formula through a piecewise integration of the time rate derivative of the Euler equations around spatially translated control volumes (i.e., defined by abcd) given by

$$\left.\frac{\partial^2 U}{\partial t^2}\right|_{\substack{\text{INV}\\ \text{E}}} = \frac{1}{\mathcal{V}} \int_{\text{abcd}} \frac{\partial}{\partial t}\left(\frac{\partial F_1}{\partial x} + \frac{\partial G_1}{\partial y}\right) d\mathcal{V} \tag{14}$$

These steps are identical to those taken by Ni for the solution of the Euler equations. One extra step is now added to the numerical approach to include the viscous terms of the Navier-Stokes equations. The first-order changes in time of the flow variables at the computational nodes due to the viscous terms are calculated from an integration of the shear stress and conduction terms around the same spatially translated control volumes that are used to calculate the second-order time rate changes (i.e., abcd).

$$\left.\frac{\partial U}{\partial t}\right|_{\substack{\text{VIS}\\ \text{E}}} = \frac{1}{\mathcal{V}} \int_{\text{abcd}} \left(\frac{\partial F_2}{\partial x} + \frac{\partial G_2}{\partial y}\right) d\mathcal{V} \tag{15}$$

These time rate changes due to the viscous effects are added to the combined first- and second-order inviscid time rate changes just prior to updating of the flow variables. The flow variables are then updated in time and the multiple-grid alogrithm[8] which is based solely on the Euler equations is initiated.

The shear stress and conduction terms at the primary control volume centers a, b, c, and d are obtained using appropriate first-order backward or forward differences at the computational node E which are subsequently applied to points, a, b, c, and d prior to integration. For example, the x- and y-axial velocity derivatives at point b are obtained from first-order forward and backward differences, respectively, at E:

$$\frac{\partial u}{\partial x} = \frac{1}{(x_I y_J - y_I x_J)}(y_J u_I - y_I u_J)$$

$$\frac{\partial u}{\partial y} = \frac{1}{(x_I y_J - y_I x_J)}(x_I u_J - x_J u_I) \tag{16}$$

where

$$x_I = x_F - x_E \qquad x_J = x_E - x_B$$

$$y_I = y_F - y_E \qquad y_J = y_E - y_B$$

$$u_I = u_F - u_E \qquad u_J = u_E - u_B$$

Similarly, the x- and y-velocity derivatives at point c are obtained from first-order backward differences at E. In this approach, the result of the integration of the stress and conduction terms around the control volume abcd is similar to a Laplacian 5-point finite-difference operator that is formally second-order accurate. This approximation is consistent with the finite-difference diffusion operators found in differential boundary-layer procedures and is consistent with the domain of influence of the inviscid operators in the present approach.

Turbulence Model Implementation

The Baldwin-Lomax algebraic turbulence model[16] has been implemented into the present solution procedure using a body normal grid. In previous applications[4,6] of the Baldwin-Lomax scheme for Navier-Stokes analyses, the eddy viscosity of the flow has been calculated directly on the computational mesh. In order to be consistent with boundary-layer theory, which is solved along lines perpendicular to the surface, a body normal coordinate system has been used in the present Navier-Stokes scheme to implement the Baldwin-Lomax turbulence model. The intersection points of the body normal grid and the computational grid are calculated and stored prior to the time-marching scheme. A small amount of additional calculational time is required to interpolate the flow variables and vorticity from the computational grid to the body normal grid and then interpolate the eddy viscosity distribution back from the body normal grid onto the computational grid. The advantage of the body normal grid implementation of the Baldwin-Lomax model is that it is not only consistent with boundary-layer theory, but the eddy viscosity can be computed from the wall to the edge of the computational mesh without having to make any *a priori* estimate of the location of the edge of the viscous layer, as has been done in other Navier-Stokes analyses. This increases the accuracy of the turbulence model particularly in regions of the flow where the boundary layer becomes quite thick and allows the model to distinguish where and how the eddy viscosity should decrease away from the wall in the outer layer. After the Navier-Stokes calculation is complete, the body normal grid is also very useful for obtaining velocity profile information as well as the integral quantities such as momentum and displacement thickness, as will be demonstrated in the section titled "Results and Discussion." It has been found through numerical experimentation that the eddy viscosity need not be calculated every time step, which generally must be performed when using the time-dependent two equation turbulence models. The eddy viscosity in the present Navier-Stokes algorithm is recalculated every 20th time step.

Numerical Smoothing

Numerical experiments have shown that when the computational grid is sufficiently fine for a given problem, the present Navier-Stokes technique does not require any artificial viscosity in the form of numerical smoothing to prevent oscillations in the flowfield. For typical cascade geometries, however, the computational time and computer storage required to obtain solutions using computational grids that are fine enough to alleviate the need for numerical smoothing are too great. A detailed study of the present numerical procedure on typical cascade geometries has been conducted to define a numerical smoothing strategy that does not contaminate the velocity or temperature profiles but yet maintains stability in regions of high gradients and relatively coarse grid spacing. A combination of second and fourth difference numerical smoothing similar to that presented in Refs. 4 and 18 is used to eliminate oscillations. In the present procedure, an artificial diffusion operator given by

$$D_k(U) = \psi_2 \left(\frac{P_{k-1} - 2P_k + P_{k+1}}{P_{k-1} + 2P_k + P_{k+1}} \right) (\bar{U}_{k-1} - 2\bar{U}_k + \bar{U}_{k+1})$$

$$- \psi_4 (\bar{U}_{k-2} - 4\bar{U}_{k-1} + 6\bar{U}_k - 4\bar{U}_{k+1} + \bar{U}_{k+2})$$

where

$$\bar{U} = U + \Delta U \tag{17}$$

$$\psi_2 = 0.25\, g_2(N) \text{ and } \psi_4 = 0.004\, g_4(N)$$

is added to the right-hand side of the numerical approximation to Eq. (1). Smoothing in the form of Eq. (17) is performed on $U = \rho,\ \rho u,\ \rho v$, and E along the streamwise (where $k = \mathrm{I}$) and tangential (where $k = \mathrm{J}$) computational lines. Smoothing of the flow variables within U is based upon the variables plus their total time rate changes ΔU with the exception that the smoothing of E is based upon $E + P$ plus their total time rate changes. The study has shown that both the second and fourth difference numerical smoothing of the velocity components (i.e., ρu and ρv) must be reduced to zero in both directions as the solid boundary is approached in order to maintain agreement with boundary-layer theory. Numerical tests have shown that the numerical smoothing of the density and energy does not need to be reduced to zero, however, thereby alleviating oscillations in the pressure field. The functions $g_2(N)$ and $g_4(N)$ are exponential decay functions which are used to reduce the second and fourth difference smoothing, respectively, of ρu and ρv to zero from the outer computational boundary to the wall. These functions are not used in the smoothing of the density and energy. The $g_2(N)$ and $g_4(N)$ functions are somewhat arbitrary and are defined to approach zero quickly from the edge of the boundary layer to the wall. In supersonic regions of the flow, it is necessary to reduce ψ_4 and raise ψ_2, especially in high gradient regions since the fourth difference smoothing has a destabilizing effect. The solutions shown in the section on results demonstrate the accuracy that is obtainable with boundary-layer theory using the present smoothing techniques.

Computational Grid for Cascades

A modified C grid generation procedure has been developed for cascades that greatly reduces grid skewing in the mid passage region thereby reducing truncation errors of the numerical scheme and errors associated with numerical smoothing. This procedure, developed in collaboration with Dannenhoffer,[13] is based upon the technique presented by Sorenson[14] and Steger and Sorenson.[15] The Dirichlet boundary condition typically used in the midgap region of cascades has been replaced with a periodic boundary condition and the outer boundary is solved in the same fashion as the interior points. The number of points at the upstream boundary is prescribed and held fixed during the computation. Solution of the outer boundary is performed by differencing the Poisson equations across the periodic boundary and setting the weighting factors associated with the outer boundary on the right-hand side of the Poisson equations to zero, except near the upstream boundary where they are chosen so as to vary the grid spacing smoothly from that at the upstream boundary. An iterative, implicit successive line relaxation scheme is used to solve the tridiagonal equation set. Figures 2a and 2b show a comparison between a standard C grid which has been used in several investigations[4-6] for cascade flows and the new modified C grid. The periodic boundary condition on the midgap boundary allows the computational mesh to adjust itself in both directions from the initial guess in order to make the mesh as orthogonal as possible in this region. As a result, the metrics of the computational grid remain continuous

across the periodic boundary, which should reduce the truncation error of the Navier-Stokes scheme. In addition, it has been found that the numerical errors associated with numerical smoothing on skewed grids are reduced considerably.

In the generation of computational grids for viscous calculations, an algebraically generated grid is patched into a relatively coarse Euler C grid near the airfoil surface and along the wake centerline. The patched viscous grid is determined by adding and redistributing mesh points along the original tangential grid lines of the Euler mesh using a logarithmic stretching formula which ensures a constant spacing at the wall, which is typically 10^{-4} of the airfoil axial chord, as well as continuous spacing at the outer edge of the patched grid. By generating the viscous grid in this manner, much less computational time is required by the Poisson solver and much more control of the grid point distribution in the viscous part of the flowfield is obtained. The modified C grid is very general, as shown in the following section, and can be used for cascades over a wide range of turning and solidity.

Results and Discussion

The previously described Navier-Stokes solution procedure has been tested on several cascade configurations. A model problem in which the computational grid spacing is sufficiently fine to alleviate the need for any explicit numerical smoothing has been used extensively to test the accuracy of the present procedure. The results of this model problem for transitional flow with heat transfer are presented. A turbine cascade with fully turbulent subsonic flow, a compressor cascade with transitional transonic flow, and a turbine cascade with transitional separated flow are also presented as a demonstration of the accuracy of the present technique for typical cascade configurations.

Model Problem

Chima and Johnson[11] presented results for the laminar flow over a 10% circular arc cascade with a unit chord and a gap/chord ratio of 2.0 at an upstream chord Reynolds number of 8.1×10^3. The present Navier-Stokes scheme has been tested on this test case and found to give excellent agreement with their results as well as with boundary-layer theory. A similar test case for transitional flow with heat transfer has been calculated for the same geometry but at a much higher Reynolds number. In this case, the chord Reynolds number based on the upstream conditions was 10^5, the Prandtl and turbulent Prandtl numbers were 0.72 and 0.95, respectively, and the inlet and exit Mach numbers were 0.5. A 125×33 point grid was used in this calculation where the minimum Δy/chord at the wall was 3.125×10^{-4} and the minimum Δx/chord at the leading edge of the cascade was 7.5×10^{-3}. Approximately 15 grid points were located in the boundary-layer region. The grid was refined at the leading edge of the cascade in order to resolve the high streamwise gradients in the flow near the stagnation point without the use of any numerical smoothing. Two levels of multiple grid were used in addition to the fine grid solution to accelerate convergence to steady state. The inlet total pressure and average air angle, as well as the exit static pressure, were held constant during the calculation. A tangency condition was enforced on the upper (midchannel) boundary as well as the lower boundary upstream of the cascade leading edge located at $x=0.0$. A no-slip boundary condition was used on the cascade wall as well as the splitter plate downstream of the blade. A wall temperature 50% greater than the freestream total temperature was specified and held constant during the calculation. Instantaneous transition from laminar to turbulent flow was specified at $x=0.5$ (midchord) and held fixed during the calculation. The calculation was run 2000 time steps which resulted in the maximum change in the normalized mass flux ($\Delta\rho V$) to be reduced four orders of magnitude. Figures 3a and 3b show the pressure and Stanton number distributions for the circular arc cascade, respectively. The ALESEP[19] finite-difference boundary-layer procedure was run using the boundary-layer edge velocity calculated from the surface pressure distribution shown in Fig. 3a as the prescribed edge condition. The boundary-layer solution was calculated using the same streamwise grid locations as prescribed in the Navier-Stokes solution. Figure 3b shows very good agreement between the present Navier-Stokes and boundary-layer results for the Stanton number. Similar agreement was found in the skin friction and displacement thickness distributions. Figures 3c and 3d show a comparison of the Navier-Stokes and boundary-layer velocity and temperature profiles at three locations along the cascade. Excellent agreement exists between the Navier-Stokes and boundary-layer solutions. This favorable comparison demonstrates that the current Navier-Stokes procedure is capable of accurately resolving thin viscous layers.

Turbine Cascade

Figure 2b shows the computational mesh used for a low pressure turbine tested experimentally by Sharma et al.[20] The inlet and exit aerodynamic conditions chosen for the numerical calculations are given in Fig. 4b. The flow was assumed to be fully turbulent. In the viscous solution, a 161×33 point mesh was used where the first grid point off the body was located 10^{-4} of the axial chord away from the surface. Since the flow was essentially adiabatic, the viscous calculation was performed with the total temperature held constant. The solution was considered to be converged when the maximum change in the normalized mass flux $\Delta\rho V$ was less than 10^{-4}. This typically reflects a reduction of at least three orders of magnitude from its initial value.

Figure 4a shows the effect of multiple grid on the convergence history for this turbine case. A viscous calculation on the fine grid shown in Fig. 2b without multiple grid took 4700 iterations to reach convergence, whereas in a similar calculation which used three levels of multiple grid in addition to the fine grid, convergence was reached in 890 iterations. Convergence was obtained 5.3 times faster for this viscous calculation through the use of three levels of multiple grid in addition to the fine grid solution. The resulting solutions of the two calculations were essentially identical demonstrating that the multiple-grid acceleration scheme has no adverse effect on the spatial accuracy.

Figure 4b shows a comparison of the predicted pressure distribution with Sharma's experimental data. The predicted pressure distribution is in excellent agreement with the experimental data. The viscous effects are relatively weak in this case as essentially the same pressure distribution was deduced from an inviscid solution. Therefore it was feasible, as in the previous model problem case, to assess the accuracy of the viscous flow solution obtained from the Navier-Stokes equations with the results of a direct calculation of the boundary-layer equations subject to the computed pressure shown in Fig. 4b. A boundary-layer solution, extending from the leading edge stagnation point to the trailing edge on the suction side of the airfoil, was calculated with the same streamwise grid as used in the Navier-Stokes solution. A small separation bubble near the leading edge prevented a similar direct boundary-layer calculation for the pressure side of the airfoil. Figure 4c shows good agreement between the predicted skin-friction distribution of the Navier-Stokes procedure with the results of a finite-difference boundary-layer solution for the suction side of the turbine blade. The oscillations in the skin-friction distribution in the leading and trailing edge region are probably due to the truncation error that results from the relatively coarse streamwise grid spacing. These oscillations could be eliminated with either a refinement of the computational mesh in these regions or with an increase in the fourth difference smoothing; however, the agreement with the

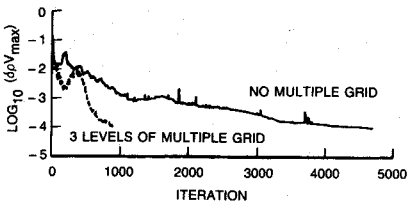

Fig. 4a Effect of multiple grid on convergence history for turbine cascade.

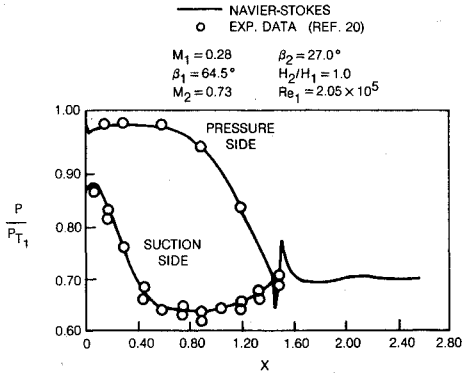

Fig. 4b Predicted pressure distribution for turbine cascade.

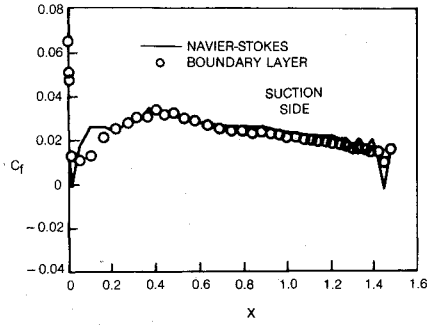

Fig. 4c Predicted skin-friction distribution for turbine cascade.

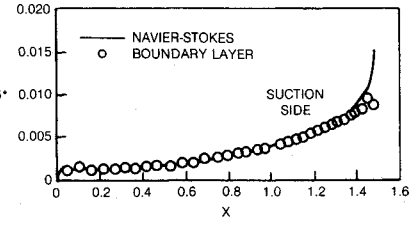

Fig. 4d Predicted displacement thickness distribution for turbine cascade.

boundary-layer solution has been found to deteriorate correspondingly with higher levels of numerical smoothing. Figure 4d shows a similar comparison between the Navier-Stokes solution and the boundary-layer solution for the displacement thickness on the suction side of the airfoil. Excellent agreement exists between the two solutions demonstrating that the Navier-Stokes technique is capable of predicting boundary-layer integral quantities with high accuracy. Very good agreement also exists between the predicted velocity profiles of the Navier-Stokes and boundary-layer solutions. Significant effort has been required in this case, and the two cases to be discussed next, in order to reduce the numerical smoothing coefficients such that favorable comparison could be obtained with the results from attached boundary-layer theory. A critical step that has been found in this investigation is that the smoothing of the velocity components must be reduced to zero in the viscous layer in order to obtain consistent results with boundary-layer theory.

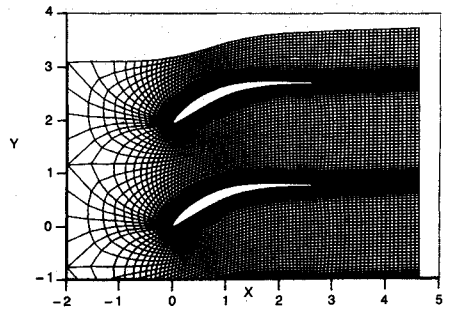

Fig. 5a Computational grid for compressor cascade.

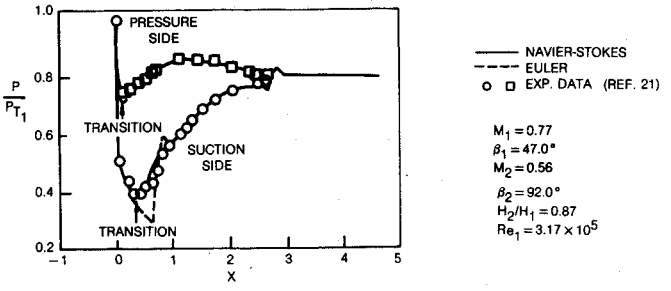

Fig. 5b Predicted pressure distribution for compressor cascade.

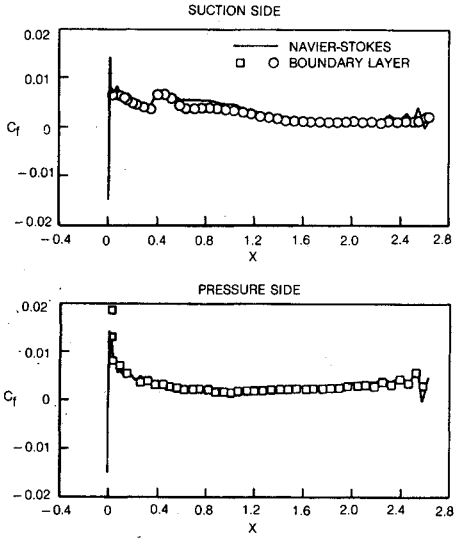

Fig. 5c Predicted skin-function distribution for compressor cascade.

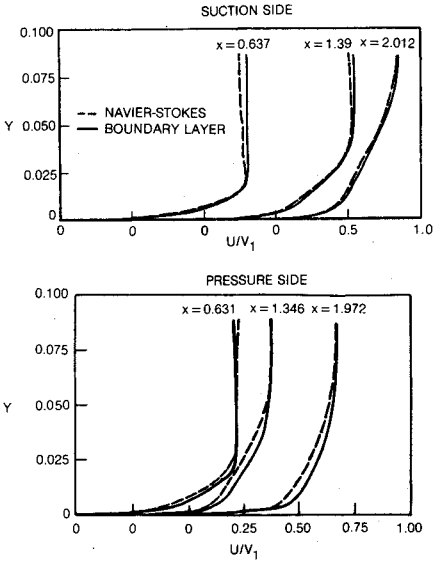

Fig. 5d Predicted velocity profile for compressor cascade.

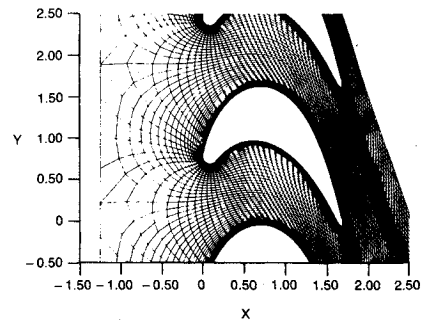

Fig. 6a Computational grid for turbine cascade.

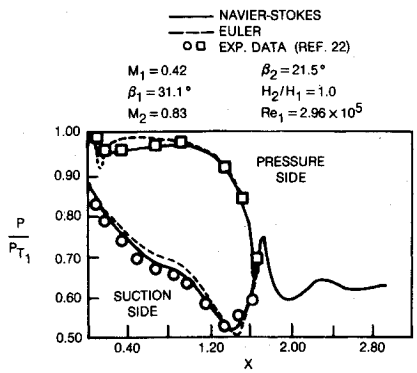

Fig. 6b Predicted pressure distribution for turbine cascade.

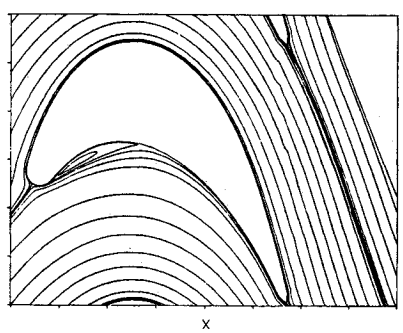

Fig. 6c Predicted streamline pattern for separated turbine cascade.

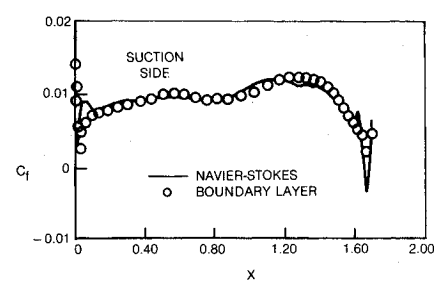

Fig. 6d Predicted skin-friction distribution for separated turbine cascade.

Compressor Cascade

Calculations have also been performed for the transonic compressor blade tested experimentally by Stephens and Hobbs.[21] As in the previous turbine example, a 161×33 point mesh, shown in Fig. 5a, was used in the viscous solution whereas a 161×17 point mesh was used in the inviscid calculation. Three levels of multiple grid were run in addition to the fine grid solution in both the viscous and inviscid calculations. The viscous solution converged ($\Delta\rho V_{max} < 10^{-4}$) in 1380 time steps, whereas the inviscid solution converged in 290 time steps using the same criteria. Transition was held fixed at the minimum pressure point on each side of the airfoil just aft of the leading edge. The inlet and exit aerodynamic conditions chosen for this cascade are given in Fig. 5b. Figure 5b shows the comparison between the viscous and inviscid predicted pressure distributions with the experimental data. Excellent agreement exists between the viscous solution and the experimental data, whereas the inviscid solution predicts a strong shock on the suction side of the airfoil which is not observed in the experimental data. The interaction between the viscous and inviscid flows in the transonic region of this cascade is quite strong as shown in Fig. 5b by the large difference between the viscous and inviscid solutions in this region. In order to evaluate the accuracy of the Navier-Stokes solution, a finite-difference boundary-layer solution was calculated between the leading edge stagnation point and the trailing edge on each side of the airfoil. As in the previously described cases, the predicted pressure distribution of the Navier-Stokes solution was used as the input edge condition for the boundary-layer calculations. The streamwise grid points defined in the Navier-Stokes solution were used in the boundary-layer calculations. Figure 5c shows a comparison between the predicted skin-friction distribution of the Navier-Stokes and boundary-layer solutions. Very good agreement exists between the two solutions. Figure 5d shows the predicted velocity profiles of the Navier-Stokes and boundary-layer solutions at three positions along each side of the airfoil. Good agreement exists between the Navier-Stokes and boundary-layer velocity profile solutions, thereby demonstrating that the present method is simultaneously capable of capturing small scale viscous flow near the surface as well as the global inviscid flow. Comparison of the Navier-Stokes velocity profiles, such as shown in Fig. 5d, and temperature profiles with boundary-layer theory is greatly expedited through the use of the body normal grid previously discussed.

Turbine Cascade With Separated Flow

A case which demonstrates the ability of the current Navier-Stokes procedure to predict flows with significant separation is the subsonic turbine cascade tested experimentally by Stoeffler et al.[22] The 161×33 point grid shown in Fig. 6a was used in the viscous calculation whereas a 161×17 point mesh was used for the inviscid calculation. Both calculations were run with three levels of multiple grid in addition to the fine grid solution. The viscous solution converged in 1500 time steps whereas the inviscid calculation reached convergence in 260 time steps. The flow on the suction side of the airfoil was assumed to be fully turbulent, and for the pressure side of the airfoil, where a large separated region existed, transition was held fixed at $x = 0.24$, which was determined from the empirical correlation of Roberts[23] for closed transitional separation bubbles. The inlet and exit aerodynamic conditions for this cascade are given in Fig. 6b along with the comparison between the predicted pressure distributions and the experimental data. Comparison of the predicted pressure distributions from both the Navier-Stokes and Euler analyses with the experimental data in Fig. 6b shows that the Navier-Stokes analysis has predicted correctly the change in the pressure due to the viscous effects. In this case it is quite clear that a significant inviscid-viscous interaction occurs due to the pressure side separation that affects the pressure distribution on both sides of the airfoil. The predicted streamline pattern shown in Fig. 6c clearly shows the extent of the separated flow region on the pressure side of the airfoil. A boundary-layer solution was calculated for the suction side of the turbine airfoil between the leading edge stagnation point and the trailing edge to establish the accuracy of the Navier-Stokes solution as compared with boundary-layer theory. As in the previous examples, the predicted pressure distribution of the Navier-Stokes solution was used as the input edge condition for the boundary-layer calculation. Again, the Navier-Stokes streamwise grid point locations were used in the boundary-layer calculation. Figure 6d shows a comparison of the predicted skin-friction distribution between the Navier-Stokes and

boundary-layer solutions. Good agreement exists between the two solutions. Similar agreement exists between the Navier-Stokes and boundary-layer solutions for the displacement thickness and velocity profiles as that shown in the previous examples.

Concluding Remarks

A solution technique for the Navier-Stokes equations is presented and demonstrated for cascades. This method which is based on a previously developed[8,9] explicit multiple-grid, time-marching scheme has been significantly improved through the incorporation of a new compact viscous term discretization scheme, an improved C grid generator, and the implementation of the Baldwin-Lomax turbulence model imposed along a body normal coordinate system. The accuracy of the computed solutions has been evaluated with experimental wall pressures and for attached flows, solutions of the boundary-layer equations subject to the wall pressure computed in the Navier-Stokes analysis. The results of these comparisons are quite favorable and have led to the principal conclusion of this work that the present method for solving the Navier-Stokes equations is capable of yielding accurate solutions for the flow in turbine and compressor cascades provided that the grid is sufficiently fine and that the second and fourth difference numerical smoothing for the primary variables ρu and ρv is reduced to zero in the viscous layer.

Acknowledgments

This work was supported by Pratt & Whitney Aircraft and the United Technologies Research Center under the Corporate Research Program.

References

[1]Hah, C., "A Navier-Stokes Analysis of Three-Dimensional Turbulent Flows Inside Turbine Blade Rows at Design and Off-Design Conditions," ASME Paper 83-GT-40, March 1983.

[2]Weinberg, B.C., Yang, R. J., McDonald, H., and Shamroth, S. J., "Calculation of Two- and Three-Dimensional Transonic Cascade Flow Fields Using the Navier-Stokes Equations," ASME Paper 85-GT-66, March 1985.

[3]Briley, W. R. and McDonald, H., "Solution of the Multidimensional Compressible Navier-Stokes Equations by a Generalized Implicit Method," *Journal of Computational Physics*, Vol. 24, July 1977, pp. 372-397.

[4]Chima, R. V., "Analysis of Inviscid and Viscous Flows in Cascades with an Explicit Multiple-Grid Algorithm," AIAA Paper 84-1633, June 1984.

[5]Shamroth, S. J., McDonald, H., and Briley, W. R., "Prediction of Cascade Flowfields Using the Averaged Navier-Stokes Equations," *ASME Journal of Engineering for Power*, Vol. 106, April 1984, pp. 383-390.

[6]Schafer, O., Furhauf, H., Bauer, B., Guggolz, M., and Kuster, U., "Application of a Navier-Stokes Analysis to Flows Through Plane Cascades," ASME Paper 85-GT-56, March 1985.

[7]Norton, R. J. G., Thompkins, W. T. Jr., and Haimes, R., "Implicit Finite Difference Schemes with Non-Simply Connected Grids—A Novel Approach," AIAA Paper 84-0003, Jan. 1984.

[8]Ni, R. H., "A Multiple-Grid Scheme for Solving the Euler Equations," *AIAA Journal*, Vol. 20, Nov. 1982, pp. 1565-1571.

[9]Davis, R., Ni, R. H., and Bowley, W., "Prediction of Compressible Laminar Viscous Flows Using a Time-Marching Control Volume and Multiple-Grid Technique," *AIAA Journal*, Vol. 22, Nov. 1984, pp. 1573-1581.

[10]Davis, R., "The Prediction of Compressible, Viscous Secondary Flows in Channel Passages," Ph.D. dissertation, University of Connecticut, Storrs, CT, July 1982.

[11]Chima, R. V. and Johnson, G. M., "Efficient Solution of the Euler and Navier-Stokes Equations with a Vectorized Multiple-Grid Algorithm," *AIAA Journal*, Vol. 23, Jan. 1985, pp. 23-32.

[12]Johnson, G., "Multiple-Grid Convergence Acceleration of Viscous and Inviscid Flow Computations," NASA TM-83361, April 1983.

[13]Dannenhoffer, J. F., private communication, 1984.

[14]Sorenson, R. L., "A Computer Program to Generate Two-Dimensional Grids About Airfoils and Other Shapes by the Use of Poisson's Equation," NASA TM-81198, May 1980.

[15]Steger, J. L. and Sorenson, R. L., "Automatic Mesh-Point Clustering Near a Boundary in Grid Generation with Elliptic Partial Differential Equations," *Journal of Computational Physics*, Vol. 33, No. 3, Dec. 1979, pp. 405-410.

[16]Baldwin, B. S. and Lomax, H., "Thin-Layer Approximation and Algebraic Model for Separated Turbulent Flows," AIAA Paper 78-257, Jan. 1978.

[17]Richtmyer, R. D. and Morton, K. W., *Difference Methods for Initial Value Problems*, Wiley, New York, 1967.

[18]Jameson, A. and Baker, T. J., "Solution of the Euler Equations for Complex Configurations," AIAA Paper 83-1929, July 1983.

[19]Davis, R. L., Vatsa, V. N., and Carter, J. E., "ALESEP: A Computer Program for the Analysis of Airfoil Leading Edge Separation Bubbles," NASA CR-172310, April 1984.

[20]Sharma, O. P., Kopper, F. C., Knudsen, L. K., and Yustinich, J. B., "Low-Pressure Turbine Subsonic Cascade Technology Report," NASA CR-165592, Jan. 1982, p. 67.

[21]Stephens, H. E. and Hobbs, D. E., "Design and Performance Evaluation of Supercritical Airfoils for Axial Flow Compressors," NAVAIR Rept. FR11455, June 1979.

[22]Stoeffler, R., Dring, R. P. and Kopper, F., "An Experimental Study of Cascade Performance for a High Pressure Turbine," United Technologies Internal Rept. UTRC 77-111, Oct. 1977.

[23]Roberts, W. B., "Calculation of Laminar Separation Bubbles and Their Effect on Airfoil Performance," AIAA Paper 79-0285, Jan. 1979.